Wrench Capability Analysis of a Cooperative Multi-UAV Parallel Robot with Rigid Links

Shiyu Liu, Stéphane Caro, Abdelhamid Chriette, Isabelle Fantoni

Wrench Capability Analysis of a Cooperative Multi-UAV Parallel Robot with Rigid Links

Shiyu Liu
Nantes Université
Ecole Centrale Nantes
CNRS, LS2N, UMR 6004
1 rue de la Noë
44321, Nantes, France
Email: shiyu.liu27@outlook.com

Stéphane Caro*
Nantes Université
Ecole Centrale Nantes
CNRS, LS2N, UMR 6004
1 rue de la Noë
44321, Nantes, France
Email: stephane.caro@ls2n.fr

Abdelhamid Chriette
Nantes Université
Ecole Centrale Nantes
CNRS, LS2N, UMR 6004
1 rue de la Noë
44321, Nantes, France
Email: abdelhamid.chriette@ls2n.fr

Isabelle Fantoni
Nantes Université
Ecole Centrale Nantes
CNRS, LS2N, UMR 6004
1 rue de la Noë
44321, Nantes, France
Email: isabelle.fantoni@ls2n.fr

ABSTRACT

The wrench capability analysis of an aerial parallel robot named Flying Parallel Robot (FPR), which involves multiple Unmanned Aerial Vehicles (UAVs) cooperatively supporting a moving platform with rigid links, is investigated in this paper. The concept of the Available Thrust Set (ATS) associated with a quadrotor system is introduced, which allows to determine the admissible range of thrust forces generated by a quadrotor actuator given its actuation limits. Under the quasi-static equilibrium condition, the Available Wrench Set (AWS) of the platform is calculated, through the derivation of a wrench matrix that relates the thrust force vectors to the wrench exerted on the platform. A quantitative metric, referred to as capacity margin, is adopted to evaluate the wrench capability of the system with certain robot configurations. The detailed analysis is showcased through several case studies and validated in both ROS simulations and experiments conducted on a real robot.

1 INTRODUCTION

Wrench capability analysis is a classical method to analyze and characterize the robot's manipulation capacity, which has been extensively studied for the Cable-Driven Parallel Robots (CDPRs), such as to determine its wrench-feasible workspace [1] or to analyze the feasibility of specific manipulation tasks [2]. The wrench capability analysis of a robot aims to define the available wrench (i.e., force and moment) the robot can generate on its end-effector while considering the actuator torque limits.

*Address all correspondence to this author.

The wrench analysis is also an important topic in legged robots for the contact/motion planning based on the computation of Actuation Wrench Polytope (AWP) and Feasible Wrench Polytope (FWP) as in [3, 4, 5, 6, 7, 8], because the determination of footprints that remains in the feasible wrench workspace is crucial for stable locomotion of such robots. Therefore, the computed FWP can be employed to an optimization process for footholds (contact points) selection [4, 7, 8], trajectory/motion planning [3, 5, 7] and optimal control [6]. Similar problems have equivalently been investigated in research related to robotic grasping, a domain that has flourished much earlier [9, 10, 11]. In these works, the notion of Grasp Wrench Space (GWS) is applied, indicating the set of wrenches that can be applied to an object by a grasp given limits on the contact normal forces [9]. A GWS can be created by the combination of friction cones on the contacts, called Cone Wrench Space (CWS), within which a force in each contact can be applied to the object to perform a stable grasp. The GWS can therefore be employed to analyse the grasping stability.

More recently, designs based on a parallel mechanical architecture have been proposed where a moving platform (or a payload) is collectively supported by multiple UAVs using cables [12, 13, 14] or rigid links [15, 16, 17]. Such robots have shown their potential in accomplishing various manipulation tasks due to higher payload capacity and better manipulability, which might largely extend the application fields of the flying robots.

In systems involving multiple Unmanned Aerial Vehicles (UAVs) connected with cables such as Aerial Cable-Towed Systems (ACTS) [13, 14], the actuation limits are due to the limited thrusts the UAVs can generate. In these works, quadrotors are connected to a payload (or a moving-platform) by cables, and the system is analogous to CDPR with the difference of that the original fixed actuators are replaced by mobile UAVs. Thus, the available wrench set (AWS) can be calculated based on the cable tension bounds. For multi-UAV systems where UAVs are rigidly connected to the platform such as [15, 16], they often use spherical joint connections which allow to consider UAVs as rotating thrust generator in 3-dimensional space. The wrench capability analysis for such systems is therefore finding the linear mapping from the UAVs' limited thrusts (or equivalently limited motor speeds) to the available wrench in the platform's configuration space, as investigated in [15, 16].

With intensive wrench capability analysis having been proposed for above-mentioned various types of parallel robots, there is a lack of in-depth wrench analysis on one special class of aerial robots, which can be summarized as cooperative multi-UAV parallel robots with rigid links where multiple UAV actuators support collectively a payload or a moving-platform by multiple rigid limbs. Whereas [15, 16] studied the wrench capability of two aerial cooperative robots with a single rigid architecture supported by multiple UAVs, this paper focuses on a more general wrench capability analysis applied to cooperative multi-UAV parallel robots by taking an example of Flying Parallel Robot (FPR), which has more degrees-of-freedom (DoFs) than the robots studied previously.

The FPR, initially proposed by [17], then modified and improved by [18], is a design where multiple UAVs are connected to a moving-platform with multiple articulated limbs. As an analogy to the parallel mechanism, the FPR can drive the platform with better mobility in particular the rotational movements by additional DoFs in passive kinematic chains. A working prototype of the analyzed FPR is shown in Fig. 1. This kind of aerial robots has the potential of accomplishing a variety of aerial manipulation tasks, as investigated in [19, 20]. However, the wrench capability of the FPR is not studied in the previous works, which is essential to determine the range of wrenches that the robot can exert for a manipulation task.

This paper presents a detailed analysis of the wrench capability of FPR, which is elaborated by firstly introducing Available Thrust Set (ATS) depicting the admissible thrust forces generated by the quadrotor actuators. The Available Wrench Set (AWS) of the moving-platform is then defined based on the force and moment transmissions from multiple limbs to the platform in the quasi-static equilibrium condition. The rest of the paper is organized as follows. The FPR system is firstly described in Section 2. Then a detailed analysis of the wrench capability of the FPR is presented in Section 3. Several case studies are showcased in Section 4. Finally, simulation and experimental results are given and discussed in Section 5.

2 SYSTEM DESCRIPTION

The Flying Parallel Robot (FPR) studied within the scope of this paper is composed of multiple quadrotor UAVs collectively supporting a moving-platform (MP) with rigid legs and passive joints. As shown in Fig. 2, one end of each leg is connected to the platform using one-DoF revolute joint. One quadrotor is attached to the other end of each limb by means of a passive spherical joint. The CoM of each quadrotor is supposed to be located at the geometric center of the spherical joint. This assumption allows to consider a cascaded system, where the dynamics of the

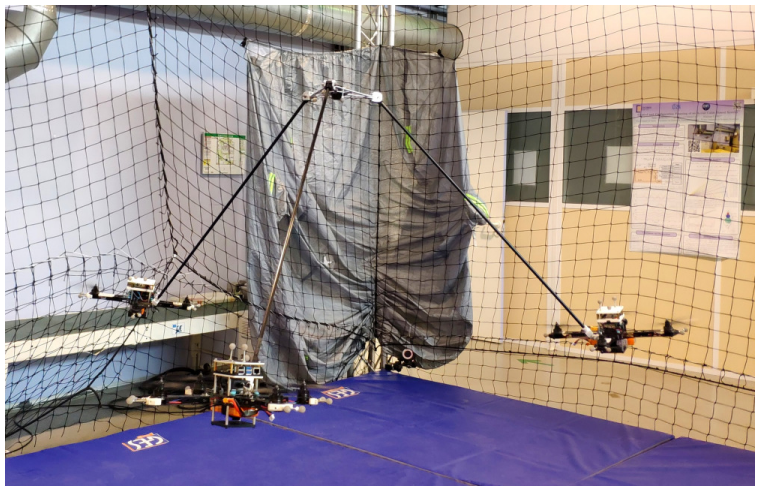

Fig. 1: A working prototype of the flying parallel robot with three quadrotor UAVs.

passive architecture is fully decoupled with the rotational dynamics of each quadrotor [17, 18]. The only actuation of the system is provided by quadrotors' thrust forces, transmitted via spherical joints to the legs, which then drive the moving platform. The minimum number of the quadrotors (and the legs) is equal to three to fully actuate the 6-dimensional pose of the platform [18]. In this paper, we focus on analyzing a typically fully-actuated FPR with three quadrotors. However, the method can be generalized to any FPR with n quadrotors and limbs.

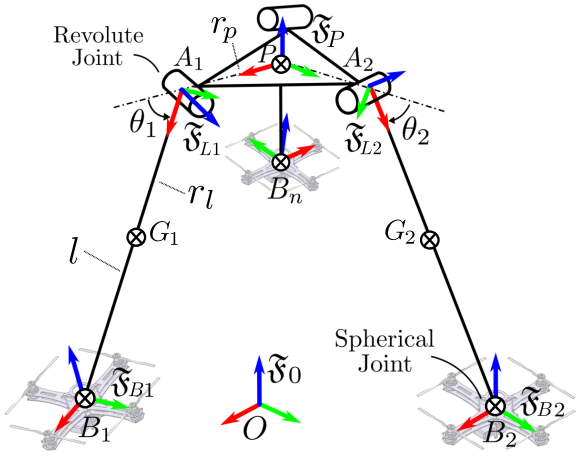

Fig. 2: General scheme of the flying parallel robot. Note that this scheme presents a generic FPR with n limbs, $n \geq 3$. The axes are defined in x-y-z order by red, green and blue arrows.

2.1 Parametrization

The geometric parameterization of a generic FPR with n quadrotors connected to n limbs is essential to formulate the methodology. Let $\mathfrak{F}_0$, $\mathfrak{F}_P$, $\mathfrak{F}_{Li}$ and $\mathfrak{F}_{Bi}$ denote respectively the global reference frame, platform's frame (attached to the platform's CoM position), leg i's frame (attached to the center of the revolute joint) and quadrotor i's body frame (attached to its CoM position), with the center of the frame given respectively by the point O, P, A_i and B_i. The CoM

position of each limb is located at point G_i. The 6-dimensional pose of the platform is defined by $\mathbf{p}_p \in \mathcal{R}^3$, $\mathbf{q}_p \in \mathcal{H}$ relative to $\mathfrak{F}_0$, where the orientation is defined by the unit quaternion with $\mathcal{H}$ being the quaternion space. It can also be defined using ZYX Euler-angle representation, by roll ϕ_p, pitch ϑ_p, and yaw ψ_p angles. θ_i denotes the revolute joint angle of the i-th leg, defined around the z axis of each leg's frame. Note that the leg is horizontally aligned with the plane of the platform when the revolute joint angle (also named as *leg angle* in the rest of the paper), θ_i is zero. All legs are supposed to have equal length l, and their CoM positions G_i are located at the same point in $\mathfrak{F}_{Li}$ with the distance of A_iG_i given by r_l. The platform's radius (i.e., distance between P and A_i) is named r_p.

Let ${}^A\mathbf{R}_B$ denote rotation matrix from $\mathfrak{F}_B$ to $\mathfrak{F}_A$. If a rotation is relative to the global reference frame $\mathfrak{F}_0$, the subscript 0 is omitted. We then use the symbols ${}^k\mathbf{f}_j$, ${}^k\boldsymbol{\tau}_j$ to represent the three-dimensional force and moment exerted on the body j, expressed in the frame k. Remark that superscripts and subscripts are listed as P (platform frame), Li (leg i's frame), and Bi (quadrotor i's body frame) to represent the frames, while bodies are described by the symbols p for the platform, li and di for the i-th limb and i-th quadrotor body. A reaction force or moment between two bodies is explicitly expressed as $\mathbf{f}_{a/b}$ or $\boldsymbol{\tau}_{a/b}$, which indicates a force/moment exerted by body a to body b.

2.2 Force and Moment Transmission

As mentioned above, each quadrotor generates a thrust force that is exclusively transmitted to the leg via spherical joint, which drives the passive architecture collectively with other quadrotors. The mechanical property of spherical joint ensures that only 3-dimensional force but no moment can be transmitted between the quadrotor and the leg. Since the connection between each leg and the moving-platform (MP) is then achieved by means of a revolute joint, an additional DoF is integrated as the rotation around the revolute joint axis. Due to the revolute-joint connection, there will be moment reaction components perpendicular to the revolute joint axis and a force reaction in a general direction (i.e., three force components and two moment components between the leg and the MP). The moment generated around the revolute joint axis (i.e., the z axis of $\mathfrak{F}_{Li}$) will not be transmitted between two bodies. The force that a quadrotor exerts at the extremity of each limb will balance the reaction force acting on the other end of the limb, which will eventually actuate the MP. While there is no moment generated at the center of the spherical joint, a resultant moment is caused at the center of revolute joint on each limb due to the force transmitted at the bottom of the leg, in which the z-axis component is not transmitted to the MP, but only serves as balancing the limb around the revolute joint.

Figure 3 shows the force and moment transmission relationship of an arbitrary leg i and the attached quadrotor i. The three-dimensional thrust force $\mathbf{f}_{ti}$ generated at the center of the spherical joint at the leg's extremity is used to balance the quadrotor's mass and the reaction force from the leg (i.e., $\mathbf{f}_{ri}$), of which the latter is the force that actuates the limb. At the revolute joint's center A_i located at the other end of the leg, a three-dimensional reaction force between the i-th limb and the MP is defined as $\mathbf{f}_{li/p}$ expressed in $\mathfrak{F}_0$. Two moment components around the x and y axes of $\mathfrak{F}_{Li}$ (i.e., two directions other than the revolute joint axis of each limb) are transmitted between the MP and the limb, which are then balanced by the resultant moment around the center of the revolute joint due to the force actuation at the bottom of the leg. However, since the resultant moment around the x axis is always null, there is no moment transmitted to the MP around the x axis of $\mathfrak{F}_{Li}$.

2.3 Static Equilibrium

Assuming that the FPR is working in quasi-static conditions where its motion is slow enough (a realistic assumption especially during the manipulation tasks), the quasi-static equilibrium of the FPR can be analyzed for which the entirety of thrust forces actuated and transmitted to the robot is used to compensate the wrench due to gravity.

Let $\mathbf{g} = [0, 0, -g]^T$ with $g = 9.81$ m/s^2 be the gravity vector. The static equilibrium of each individual body of the FPR architecture can be investigated separately, as shown in Fig. 4. The static equilibrium of forces exerted on each quadrotor is at first established

$$\mathbf{f}_{ti} + m_{di}\mathbf{g} - \mathbf{f}_{ri} = \mathbf{0} \tag{1}$$

with $\mathbf{f}_{ti}$ and m_{di} being the three-dimensional thrust force and the mass of the i-th quadrotor, $\mathbf{f}_{ri}$ the reaction force. As the spherical joint is realistically assumed to be located at the CoM of the quadrotor, the rotational motion of the

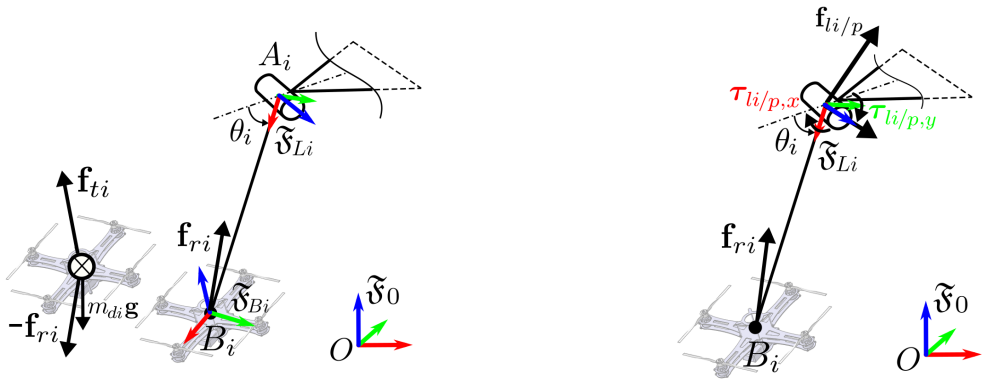

(a) Force transmitted at the center of the spherical joint

(b) Force and moment exerted at the center of the revolute joint

Fig. 3: Force and moment transmission on the i-th limb. Note that the moment components are expressed in $\mathfrak{F}_{Li}$.

quadrotor is fully decoupled with the rigid limb. The static equilibrium equation of moment for each quadrotor can therefore be neglected.

The static equilibrium regarding the force and moment on each limb can then be represented by

$$\mathbf{f}_{ri} + m_l\mathbf{g} + \mathbf{f}_{p/li} = \mathbf{0} \tag{2}$$

$$\overrightarrow{A_iB_i} \times \mathbf{f}_{ri} + \overrightarrow{A_iG_i} \times m_l\mathbf{g} + \boldsymbol{\tau}_{p/li} = \mathbf{0} \tag{3}$$

where $\mathbf{f}_{p/li}$ and $\boldsymbol{\tau}_{p/li}$ are the reaction force and moment exerted to each limb by the platform at the center of the revolute joint, and m_l is the mass of the leg supposing that all legs have equal mass.

Finally, the static equilibrium of the MP without considering any external wrench acting on the MP is given by the following relations

$$\mathbf{f}_p + m_p\mathbf{g} = \mathbf{0} \tag{4}$$

$$\boldsymbol{\tau}_p + \boldsymbol{\tau}_{g,p} = \mathbf{0} \tag{5}$$

where $\boldsymbol{\tau}_{g,p}$ is the moment caused by the mass of the platform due to the gravity if the origin of $\mathfrak{F}_P$ and CoM of the MP are not located at the same position. In this paper, $\boldsymbol{\tau}_{g,p}$ is supposed to be null. $\mathbf{f}_p$ and $\boldsymbol{\tau}_p$ are the force and moment exerted on the platform due to the actuation by all the limbs, i.e.,

$$\mathbf{f}_p = \sum_{i=1}^{n} \mathbf{f}_{li/p} \tag{6}$$

$$\boldsymbol{\tau}_p = \sum_{i=1}^{n} \boldsymbol{\tau}_{li/p} + \sum_{i=1}^{n} \overrightarrow{PA_i} \times \mathbf{f}_{li/p} \tag{7}$$

with $\mathbf{f}_{li/p} = -\mathbf{f}_{p/li}$ and $\boldsymbol{\tau}_{li/p} = -\boldsymbol{\tau}_{p/li}$ the reaction force and moment generated by the i-th limb to the platform.

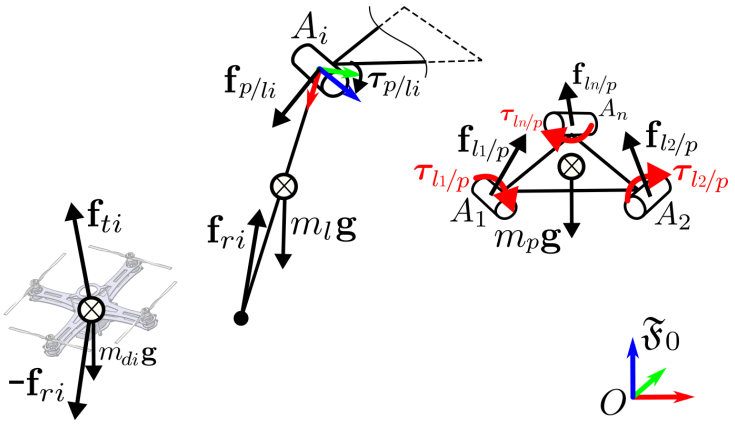

Fig. 4: Static equilibrium on the decoupled quadrotor i, limb i and the platform bodies, with forces expressed in $\mathfrak{F}_0$ and moments expressed in $\mathfrak{F}_P$.

3 WRENCH CAPABILITY

The wrench capability of FPR aims to determine the available wrench set (AWS) of the moving-platform (MP), considering the actuation limits of quadrotors, which can be characterized by the available thrust set (ATS). Unlike the cable connections in ACTS which transmit only unilateral force along the cables, the rigid limbs connecting the quadrotors to the MP in the FPR can transmit two actuation forces, respectively along the revolute-joint axis and direction of the limb, and one moment around the y axis of the limb i's frame (as detailed in Section 2.2). Therefore, the mapping from ATS of the quadrotors to the AWS of the MP is adapted to account for actual forces and moment transmitted to MP. In addition, a third component of the actuation force provided by the quadrotors (along the vector normal to the revolute-joint axis and the limb direction) is required to keep the limbs in equilibrium, which further constrains the transmission forces and moment onto the MP, which in turn affects the range of the available wrench generated on MP.

In the rest of this section, the definition of ATS of a single quadrotor is firstly elaborated, which considers the actuation limits of the quadrotor with realistic values. The wrench exerted on the platform due to the actuation from multiple limbs with quadrotors is calculated by considering the static equilibrium of each limb, which allows to determine a wrench matrix that relates the vector of quadrotor thrust forces to the generalized wrench of the robot. The mapping from the ATS to AWS is then achievable by deriving the wrench matrix. The AWS depicting the available wrench exerted on the MP is finally determined based on definition of half-spaces and hyperplanes [21]. We demonstrate the path of wrench capability analysis of the FPR from ATS to AWS by Fig. 5.

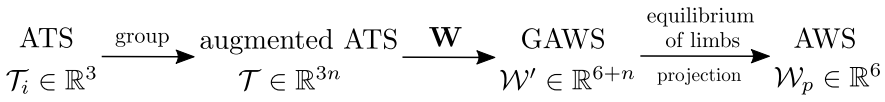

Fig. 5: Wrench capability analysis diagram from ATS to AWS.

3.1 Available Thrust Set (ATS)

As mentioned in Section 1, for systems where quadrotors are attached to the rigid link via spherical joints, the robot actuation is exclusively provided by quadrotor thrust forces. Each quadrotor can generate the thrust force within

a limited range, which is expressed in a three-dimensional space with respect to $\mathfrak{F}_0$ as

$$\mathbf{f}_{ti} = \mathbf{R}_{Bi}[0,\ 0,\ f_{ti}]^T \in \mathbb{R}^3 \tag{8}$$

where $\mathbf{R}_{bi} \in$ SO(3) is the rotation matrix representing the i-th quadrotor attitude expressed in $\mathfrak{F}_0$ and $f_{ti} \geq 0$ is the magnitude of its total thrust force. f_{ti} is constrained by a scalar value denoted by f_{max}, which represents the maximum thrust a quadrotor can generate when rotors are spinning at their maximum velocity, i.e.,

$$f_{ti} = \|\mathbf{f}_{ti}\| \leq f_{max} \tag{9}$$

Furthermore, the rotation of the quadrotor around the spherical joint is constrained by its mechanical stops, which introduces the additional constraints on the rotational movement of each quadrotor. This results in a cone constraint on the three-dimensional thrust force vector, which can be depicted as

$$\mathbf{k}^T\mathbf{f}_{ti} \geq \|\mathbf{f}_{ti}\| \cos\gamma_{max} \tag{10}$$

where $\gamma_{max} \in \mathbb{R}$, $0 < \gamma_{max} < \pi/2$ is the maximum rotation angle of the i-th quadrotor about its roll and pitch axes, $\mathbf{k} = [0, 0, 1]^T$ represents the z axis of the global frame $\mathfrak{F}_0$. Therefore, the available thrust set (ATS) of a single quadrotor taking into account these realistic constraints can be finally described by a continuous space, denoted as the available thrust space (ATS),

$$\mathcal{T}_i = \{\mathbf{f}_{ti} \in \mathbb{R}^3 \mid \mathbf{k}^T\mathbf{f}_{ti} \geq \|\mathbf{f}_{ti}\| \cos\gamma_{max},\ \|\mathbf{f}_{ti}\| \leq f_{max}\} \tag{11}$$

This space is further discretized by selecting a finite number of vertices on the surface, to create a convex polytope (see Appendix) representing the ATS. In what remains, the discretized ATS is denoted as $\mathcal{T}_i$ without distinguishing it from its continuous representation given by Eq. (11), but the expression of discretized ATS can be defined using half-spaces as

$$\mathcal{T}_i = \{\mathbf{f}_{ti} \in \mathbb{R}^3 \mid \mathbf{A}_{ti}\mathbf{f}_{ti} \leq \mathbf{b}_{ti}\} \tag{12}$$

where $\mathbf{A}_{ti} \in \mathbb{R}^{n_v \times 3}$, $\mathbf{b}_{ti} \in \mathbb{R}^{n_v}$ define the inequality constraints in Eq. (11) discretized by n_v vertices. We assume that all the quadrotors have equal ATS, so expressions of $\mathbf{A}_{ti}$ and $\mathbf{b}_{ti}$ are unique for all the quadrotors.

Then, by combining the ATS of multiple quadrotors, an augmented ATS (denoted by $\mathcal{T}$) can be defined as follows

$$\mathcal{T} = \{\mathbf{f}_t \in \mathbb{R}^{3n} \mid \mathbf{A}_t\mathbf{f}_t \leq \mathbf{b}_t\} \tag{13}$$

where $\mathbf{A}_t \in \mathbb{R}^{n \cdot n_v \times 3n}$ and $\mathbf{b}_t \in \mathbb{R}^{n \cdot n_v}$ are augmented matrix and vector for defining the inequality constraints, i.e.,

$$\mathbf{A}_t = \begin{bmatrix} \mathbf{A}_{t1} & \mathbf{0}_{n_v\times 3} & \cdots & \mathbf{0}_{n_v\times 3} \\ \mathbf{0}_{n_v\times 3} & \mathbf{A}_{t2} & \cdots & \mathbf{0}_{n_v\times 3} \\ \vdots & \vdots & \ddots & \vdots \\ \mathbf{0}_{n_v\times 3} & \mathbf{0}_{n_v\times 3} & \cdots & \mathbf{A}_{tn} \end{bmatrix}, \quad \mathbf{b}_t = \begin{bmatrix} \mathbf{b}_{t1} \\ \mathbf{b}_{t2} \\ \vdots \\ \mathbf{b}_{tn} \end{bmatrix} \tag{14}$$

3.2 Wrench on the Platform

The wrench exerted on the platform, denoted by $\mathbf{w}_p = [\mathbf{f}_p^T, {}^P\boldsymbol{\tau}_p{}^T]^T \in \mathbb{R}^6$, is due to the actuation of quadrotors (i.e., thrust forces of quadrotors) and transmission of force and moment via the limbs. Note that the force is expressed in $\mathfrak{F}_0$ while the moment is with respect to the platform's body-fixed frame. Assuming that the robot is performing in quasi-static condition, the wrench on the platform can be derived by considering the static equilibrium equations of the quadrotors and limbs presented in Section 2.3.

We know that the force and moment exerted on the platform by each limb, i.e., $\mathbf{f}_{li/p}$ and $\boldsymbol{\tau}_{li/p}$, are opposite of $\mathbf{f}_{p/li}$ and $\boldsymbol{\tau}_{p/li}$, whose expressions can be derived from Eqs. (1)–(3) as

$$\mathbf{f}_{li/p} = \mathbf{f}_{ti} + (m_{di} + m_l)\mathbf{g} \tag{15}$$

$$\boldsymbol{\tau}_{li/p} = \overrightarrow{A_iB_i} \times (\mathbf{f}_{ti} + m_{di}\mathbf{g}) + \overrightarrow{A_iG_i} \times m_l\mathbf{g} \tag{16}$$

According to the force and moment transmission rules described in Section 2.2, we can rewrite Eq. (16) to be expressed in $\mathfrak{F}_{Li}$ such that only x and y-axis components of the moment are transmitted between the MP and the i-th limb, i.e.,

$${}^{Li}\boldsymbol{\tau}_{li/p} = \left[{}^{Li}\tau_{li/p,x},\, {}^{Li}\tau_{li/p,y},\, {}^{Li}\tau_{li/p,z}\right]^T \tag{17}$$

with ${}^{Li}\tau_{li/p,z} = 0$. The x and y-axis components of ${}^{Li}\boldsymbol{\tau}_{li/p}$ are given as

$${}^{Li}\tau_{li/p,x} = \mathbf{i}_{Li}^T \cdot {}^{Li}\left[\overrightarrow{A_iB_i} \times (\mathbf{f}_{ti} + m_{di}\mathbf{g}) + \overrightarrow{A_iG_i} \times m_l\mathbf{g}\right] \tag{18}$$

and

$${}^{Li}\tau_{li/p,y} = \mathbf{j}_{Li}^T \cdot {}^{Li}\left[\overrightarrow{A_iB_i} \times (\mathbf{f}_{ti} + m_{di}\mathbf{g}) + \overrightarrow{A_iG_i} \times m_l\mathbf{g}\right] \tag{19}$$

with $\mathbf{i}_{Li}$, $\mathbf{j}_{Li}$ being the unit vectors of x and y axes of $\mathfrak{F}_{Li}$. Note that Eq. (18) is always null because $\overrightarrow{A_iB_i}$ (and $\overrightarrow{A_iG_i}$) is aligned with the x axis of $\mathfrak{F}_{Li}$. While the z-axis component of ${}^{Li}\boldsymbol{\tau}_{li/p}$ transmitted to the MP is zero, the corresponding component of Eq. (3) expressed in $\mathfrak{F}_{Li}$ still needs to be satisfied, which yields an additional constraint given by

$$\mathbf{k}_{Li}^T \cdot {}^{Li}\left[\overrightarrow{A_iB_i} \times (\mathbf{f}_{ti} + m_{di}\mathbf{g}) + \overrightarrow{A_iG_i} \times m_l\mathbf{g}\right] = 0 \tag{20}$$

where $\mathbf{k}_{Li}$ is the z-axis unit vector of $\mathfrak{F}_{Li}$. Eq. (20) can be rewritten in another form as

$$\mathbf{k}_{Li}^T \cdot {}^{Li}(\overrightarrow{A_iB_i} \times \mathbf{f}_{ti}) + \mathbf{k}_{Li}^T \cdot {}^{Li}\big(\overrightarrow{A_iB_i} \times m_{di}\mathbf{g} + \overrightarrow{A_iG_i} \times m_l\mathbf{g}\big) = 0 \tag{21}$$

of which the first term can be seen as a virtual actuation moment exerted on the revolute joint of the limb due to the quadrotor thrust force, defined as ${}^{Li}\tau_{li} := \mathbf{k}_{Li}^T \cdot {}^{Li}(\overrightarrow{A_iB_i} \times \mathbf{f}_{ti})$, while the second term is a constant moment due to the gravity, denoted by ${}^{Li}\tau_{g,li}$. Note that $\overrightarrow{A_iB_i}$ and $\overrightarrow{A_iG_i}$ are vectors aligned with the x axis of $\mathfrak{F}_{Li}$. Those two vectors are denoted as $\mathbf{r}_{A_iB_i}$ and $\mathbf{r}_{A_iG_i}$ respectively, whose expressions in $\mathfrak{F}_{Li}$ take the form ${}^{Li}\mathbf{r}_{A_iB_i} = [l, 0, 0]^T$ and ${}^{Li}\mathbf{r}_{A_iG_i} = [r_l, 0, 0]^T$.

By combining the transmitted force and moment from all the limbs, the wrench exerted to the platform without any external wrench can be known. The force transmitted to the platform is computed by Eq. (6), whereas the moment exerted to the platform is known by Eq. (7), which can be expressed in $\mathfrak{F}_P$ as

$$ {}^P\boldsymbol{\tau}_p = \sum_{i=1}^{n} {}^P\mathbf{R}_{Li}\, {}^{Li}\boldsymbol{\tau}_{li/p} + \sum_{i=1}^{n} {}^P\overrightarrow{PA_i} \times {}^P\mathbf{f}_{li/p} \tag{22} $$

where ${}^P\overrightarrow{PA_i}$ is a constant vector, denoted and determined by ${}^P\mathbf{r}_{PA_i} = [r_p \cos\alpha_i,\ r_p \sin\alpha_i,\ 0]^T$, with $\alpha_i = \frac{2\pi(i-1)}{n}$ the angle between the direction of $\overrightarrow{PA_i}$ and the x-axis of $\mathfrak{F}_P$.

Finally, by replacing terms from Eqs. (15), (16), (17) in Eq. (6) and Eq. (22), one can derive the wrench acting on the MP as

$$ \mathbf{f}_p = \sum_{i=1}^{n} (\mathbf{f}_{ti} + \mathbf{f}_{g,li/p}) \tag{23} $$

$$ {}^P\boldsymbol{\tau}_p = \sum_{i=1}^{n} \Big[{}^P\mathbf{R}_{Li}\mathbf{S}_\tau [{}^{Li}\mathbf{r}_{A_iB_i}]_\times \mathbf{R}_{Li}^T + [{}^P\mathbf{r}_{PA_i}]_\times \mathbf{R}_P^T \Big] \mathbf{f}_{ti} + {}^P\boldsymbol{\tau}_{g,li/p} \tag{24} $$

where $[.]_\times$ represents the skew-symmetric matrix of a vector, $\mathbf{f}_{g,li/p}$ and ${}^p\boldsymbol{\tau}_{g,li/p}$ are constant force and moment of gravity exerted by the i-th limb to the MP due to the masses of the quadrotor and the leg. Their expressions are given by

$$ \mathbf{f}_{g,li/p} = (m_{di} + m_l)\mathbf{g} \tag{25} $$

$$ \begin{aligned} {}^P\boldsymbol{\tau}_{g,li/p} = {} & m_{di}[{}^P\mathbf{r}_{A_iB_i}]_\times {}^P\mathbf{g} + m_l[{}^P\mathbf{r}_{A_iG_i}]_\times {}^P\mathbf{g} \\ & + (m_{di} + m_l)[{}^P\mathbf{r}_{PA_i}]_\times {}^P\mathbf{g} \end{aligned} \tag{26} $$

$\mathbf{S}_\tau \in \mathbb{R}^{3\times3}$ is the moment transmission matrix of two bodies connected by revolute joint, defined as

$$ \mathbf{S}_\tau = \begin{bmatrix} 1 & 0 & 0 \\ 0 & 1 & 0 \\ 0 & 0 & 0 \end{bmatrix} \tag{27} $$

Note that the force transmission matrix associated with a revolute joint is the 3×3 identity matrix, which is apparently ignored in Eq. (23).

3.3 Wrench Matrix

The wrench matrix used to establish the relationship between the actuation vector and the wrench acting on the platform can be derived based on equations detailed in Section 3.2. The actuation vector of the FPR is composed of quadrotor thrust forces, which can be defined as

$$ \mathbf{f}_t = \left[\mathbf{f}_{t1}^T,\ \mathbf{f}_{t2}^T,\ ...,\ \mathbf{f}_{tn}^T\right]^T \in \mathbb{R}^{3n} \tag{28} $$

The admissible range of each individual thrust force vector $\mathbf{f}_{ti} \in \mathbb{R}^3$ is depicted by the ATS defined in Eq. (11). By reformulating Eq. (23) and Eq. (24), one can derive the relationship between $\mathbf{f}_t$ and $\mathbf{w}_p$ written in matrix form as

$$\mathbf{w}_p = \mathbf{W}_p \mathbf{f}_t + \mathbf{c}_{g,l/p} \tag{29}$$

where $\mathbf{c}_{g,l/p} = [\mathbf{f}_{g,l/p}^T,\ {}^P\boldsymbol{\tau}_{g,l/p}^T]^T \in \mathbb{R}^6$ is the constant wrench of gravity exerted on the platform due to the masses of all the limbs, with $\mathbf{f}_{g,l/p} = \sum_{i=1}^n \mathbf{f}_{g,li/p}$ and ${}^P\boldsymbol{\tau}_{g,l/p} = \sum_{i=1}^n {}^P\boldsymbol{\tau}_{g,li/p}$, $\mathbf{W}_p \in \mathbb{R}^{6\times 3n}$ is the wrench matrix for the platform wrench that can be given by

$$\mathbf{W}_p = \begin{bmatrix} \mathbf{1}_{3\times 3} & \mathbf{1}_{3\times 3} & \cdots & \mathbf{1}_{3\times 3} \\ \mathbf{W}_{\tau_p,1} & \mathbf{W}_{\tau_p,2} & \cdots & \mathbf{W}_{\tau_p,n} \end{bmatrix} \tag{30}$$

with $\mathbf{W}_{\tau_p,i} \in \mathbb{R}^{3\times 3}$ being the sub-matrix linking the thrust force exerted at the extremity of the i-th limb to the moment of the platform, whose expression can be written as

$$\mathbf{W}_{\tau_p,i} = {}^P\mathbf{R}_{Li}\mathbf{S}_\tau[{}^{Li}\mathbf{r}_{A_iB_i}]_\times \mathbf{R}_{Li}^T + [{}^P\mathbf{r}_{PA_i}]_\times \mathbf{R}_P^T \tag{31}$$

However, the robot has more DoFs than 6-dimensional pose of the MP, i.e., each limb has one additional DoF as the rotation around the revolute joint axis that is driven by the resultant moment exerted at the center of the revolute joint around the z axis of $\mathfrak{F}_{Li}$. To find the admissible range of wrench exerted on the MP, the additional constraint on each limb detailed in Eq. (21) should be satisfied for stabilizing the leg angle of the limb in its static equilibrium. Therefore, we introduce a generalized wrench vector consisting in not only the wrench of the MP, but also the virtual moments generated around the revolute-joint axis of each limb, i.e.,

$$\mathbf{w} = \left[\mathbf{f}_p^T,\ {}^P\boldsymbol{\tau}_p^T,\ \boldsymbol{\tau}_l^T\right]^T \in \mathbb{R}^{6+n} \tag{32}$$

with $\boldsymbol{\tau}_l = [{}^{L1}\tau_{l1}, {}^{L2}\tau_{l2}, ..., {}^{Ln}\tau_{ln}]^T \in \mathbb{R}^n$, and we know from Eq. (21) that ${}^{Li}\tau_{li}$ is defined as

$${}^{Li}\tau_{li} = \mathbf{k}_{Li}^T[{}^{Li}\mathbf{r}_{A_iB_i}]_\times \mathbf{R}_{Li}^T \mathbf{f}_{ti} \tag{33}$$

By combining Eq. (29) and Eq. (33), the relationship between the thrust force vector and the generalized wrench vector of the FPR can be derived as

$$\mathbf{w} = \mathbf{W}\mathbf{f}_t + \mathbf{c}_g \tag{34}$$

in which $\mathbf{c}_g = [\mathbf{c}_{g,l/p}^T, \mathbf{0}_n^T]^T \in \mathbb{R}^{6+n}$ and $\mathbf{W} \in \mathbb{R}^{(6+n)\times 3n}$ is the generalized wrench matrix given by

$$\mathbf{W} = \begin{bmatrix} \mathbf{W}_p \\ \mathbf{W}_{\tau_l} \end{bmatrix} \tag{35}$$

with $\mathbf{W}_{\tau_l} = [\mathbf{W}_{\tau_{l1}},\ \mathbf{W}_{\tau_{l2}},\ ...,\ \mathbf{W}_{\tau_{ln}}] \in \mathbb{R}^{n\times 3n}$ the sub-matrix relating the quadrotor thrust force vector to the virtual moment generated around the revolute joint axes of the limbs. The expression of $\mathbf{W}_{\tau_{li}} \in \mathbb{R}^{n\times 3}$ for each individual limb is given as

$$\mathbf{W}_{\tau_{li}} = \begin{bmatrix} \mathbf{0}_3^T \\ \vdots \\ \mathbf{k}_{Li}^T[{}^{Li}\mathbf{r}_{A_iB_i}]_\times \mathbf{R}_{Li}^T \\ \vdots \\ \mathbf{0}_3^T \end{bmatrix} \tag{36}$$

with only the i-th row being not null.

3.4 Available Wrench Set (AWS)

The relationship between the thrust force vectors provided by the quadrotors and the wrench exerted on the MP was derived in the foregoing sections. The available wrench set (AWS) of the platform can now be found by considering the static equilibrium of each limb. We first rewrite Eq. (34) as

$$\begin{aligned} \mathbf{w} - \mathbf{c}_g &= \mathbf{W}\mathbf{f}_t \\ &= \begin{bmatrix} \mathbf{W}_1 & \mathbf{W}_2 & \cdots & \mathbf{W}_n \end{bmatrix} \begin{bmatrix} \mathbf{f}_{t1} \\ \mathbf{f}_{t2} \\ \vdots \\ \mathbf{f}_{tn} \end{bmatrix} \end{aligned} \tag{37}$$

of which the left-hand side can be seen as the admissible wrench generated on the robot without considering the constant wrench of gravity caused by the masses of the limbs.

Therefore, the available set of $\mathbf{w} - \mathbf{c}_g := \mathbf{w}' \in \mathbb{R}^{6+n}$ can be found by using the H-representation convex polytope given that each individual thrust force vector $\mathbf{f}_{ti}$ satisfies the ATS described by Eq. (12). We denote the generalized available wrench set (GAWS) of the FPR by $\mathcal{W}'$ corresponding to the admissible range of generalized wrench of the robot. It is straightforward to derive the expression of $\mathcal{W}'$ as

$$\mathcal{W}' = \{\mathbf{w}' \in \mathbb{R}^{6+n} \mid \mathbf{A}_{\mathrm{w}}\mathbf{w}' \leq \mathbf{b}_{\mathrm{w}}\} \tag{38}$$

where $\mathbf{A}_{\mathrm{w}} \in \mathbb{R}^{n \cdot n_v \times (6+n)}$ and $\mathbf{b}_{\mathrm{w}} \in \mathbb{R}^{n \cdot n_v}$ are the inequality constraints for determining the GAWS, whose expressions are

$$\mathbf{A}_{\mathrm{w}} = \mathbf{A}_t \mathbf{W}^{-1}, \quad \mathbf{b}_{\mathrm{w}} = \mathbf{b}_t \tag{39}$$

with $\mathbf{A}_t$, $\mathbf{b}_t$ defined in Eq. (14), and $\mathbf{W}^{-1}$ representing the inverse of the wrench matrix $\mathbf{W}$ when it is square (i.e., $n = 3$). It should be noted that when n is greater than 3, the robot is over-actuated and the GAWS can be computed using a more generic approach based on hyperplane shifting method. Readers are suggested to refer to [2, 22] for more details.

The GAWS mathematically expressed by Eq. (39) has over-estimated the admissible range of the wrench exerted on the platform, because additional constraints induced by the static equilibrium of the limbs should be taken into account, which is originally given in Eq. (21) and can be rewritten as

$${}^{Li}\tau_{li} + {}^{Li}\tau_{g,li} = 0 \tag{40}$$

with ${}^{Li}\tau_{g,li} = \mathbf{k}_{Li}^T \cdot \left(m_{di} [{}^{Li}\mathbf{r}_{A_iB_i}]_\times {}^{Li}\mathbf{g} + m_l [{}^{Li}\mathbf{r}_{A_iG_i}]_\times {}^{Li}\mathbf{g} \right)$. Such equality constraints can actually be represented by hyperplanes additionally constraining the GAWS as

$$\mathcal{W}' = \{\mathbf{w}' \in \mathbb{R}^{6+n} \mid \mathbf{A}_{\mathrm{w}}\mathbf{w}' \leq \mathbf{b}_{\mathrm{w}}, \mathbf{C}_{\mathrm{w}}\mathbf{w}' = \mathbf{d}_{\mathrm{w}}\} \tag{41}$$

with the constraint matrix $\mathbf{C}_{\mathrm{w}} \in \mathbb{R}^{n \times (n+6)}$ and vector $\mathbf{d}_{\mathrm{w}} \in \mathbb{R}^n$ given as

$$\mathbf{C}_{\mathrm{w}} = \begin{bmatrix} \mathbf{0}_{n \times 6} & \mathbf{1}_{n \times n} \end{bmatrix}, \mathbf{d}_{\mathrm{w}} = [{}^{l1}\tau_{g,l1}, {}^{l2}\tau_{g,l2}, \ \ldots, \ {}^{ln}\tau_{g,ln}]^T \tag{42}$$

After considering the static equilibrium constraints for all the limbs, the last n elements of $\mathcal{W}$ are set to the constant moments due to the masses of the limb, aiming at balancing all the limbs in their static equilibrium conditions. The AWS of the MP can be finally obtained by finding the projection of the first 6 elements of $\mathbf{w}'$ determined by Eq. (41) into the 6-dimensional space (for the 3-dimensional force and moment sub-spaces), i.e.,

$$\mathcal{W}_p = \{\mathbf{w}'_p \in \mathbb{R}^6 \mid \mathbf{w}'_p = [\mathbf{w}'(1), \mathbf{w}'(2), ..., \mathbf{w}'(6)]^T \text{ for } \mathbf{w}' \in \mathcal{W}'\} \tag{43}$$

After projecting $\mathcal{W}'$ to lower dimensional space to obtain $\mathcal{W}_p$, it can be reformulated using half-spaces defined as

$$\mathcal{W}_p = \{\mathbf{w}'_p \in \mathbb{R}^6 \mid \mathbf{A}_{\mathrm{w}_p}\mathbf{w}'_p \leq \mathbf{b}_{\mathrm{w}_p}\} \tag{44}$$

with $\mathbf{A}_{\mathrm{w}_p} \in \mathbb{R}^{N\times 6}$ and $\mathbf{b}_{\mathrm{w}_p} \in \mathbb{R}^N$ and N the reduced number of hyperplanes after the projection. In practice, we find the projection of $\mathcal{W}'$ into the 6-dimensional space to find $\mathcal{W}_p$ with expressions of $\mathbf{A}_{\mathrm{w}_p}$ $\mathbf{b}_{\mathrm{w}_p}$, which can be achieved using the toolbox [23].

We remark that $\mathcal{W}_p$ in Eq. (44) depicts the admissible range of $\mathbf{w}'_p = \mathbf{w}_p - \mathbf{c}_{g,l/p}$ with $\mathbf{c}_{g,l/p}$ being the gravity wrench that is due to the masses of limbs and transmitted to the MP. The admissible wrench set of the MP taking into account all the gravity wrench can be obtained by shifting the origin of $\mathcal{W}_p$ by the value $\mathbf{c}_{g,l/p}$. However, it should be noticed that $\mathbf{c}_{g,l/p}$ is a constant wrench with a given robot configuration. So an alternative solution is that $\mathbf{c}_{g,l/p}$ can be added in the gravity wrench of the platform when analyzing the static equilibrium of the MP, referred to Eq. (4) and (5). We have chosen to use the latter approach for the quantitative analysis detailed in the rest of the paper by introducing a new variable as the constant wrench of gravity due to the masses of the whole robot structure, i.e.,

$$\mathbf{c}_{g,p} = \mathbf{w}_{g,p} + \mathbf{c}_{g,l/p} \tag{45}$$

with $\mathbf{w}_{g,p} = [m_p\mathbf{g}^T, {}^P\boldsymbol{\tau}_{g,p}^T]^T \in \mathbb{R}^6$ defining the wrench of gravity due to the platform's mass. For consistency, the AWS of the platform $\mathcal{W}_p$ that defines the admissible range of $\mathbf{w}'_p$ without shifting by the value of $\mathbf{c}_{g,l/p}$ are visualized in the next section.

3.5 Capacity Margin

As investigated in [24, 13], the capacity margin (denoted by ζ) is an index for evaluating the robustness of equilibrium. It can be defined as the shortest distance from a wrench vector located in AWS that compensates any external wrench to all the facets of $\mathcal{W}_p$. This quantity measures how much available force and moment left to the platform to exert onto the environment, apart from balancing a known wrench already applied to the platform, such as the wrench of gravity due to the masses of all the limbs, quadrotors and the MP (i.e., $\mathbf{w}_p = -\mathbf{c}_{g,p}$). The capacity margin can be mathematically written as

$$\begin{aligned} \zeta &= \min(d_1, d_2, ..., d_j, ..., d_N), \\ \text{with } d_j &= \frac{-\mathbf{A}_{\mathrm{w}_p}(j,*)}{\mathbf{c}}_{g,p} - \mathbf{b}_{\mathrm{w}_p}(j)\mathbf{A}_{\mathrm{w}_p}(j,*) \end{aligned} \tag{46}$$

for j from 1 to N. $\mathbf{A}_{\mathrm{w}_p}(j,*)$ is the j-th row of the matrix $\mathbf{A}_{\mathrm{w}_p}$ and $\mathbf{b}_{\mathrm{w}_p}(j)$ is the j-th element of the vector $\mathbf{b}_{\mathrm{w}_p}$, both together factorizing the j-th hyperplane. $\|.\|$ represents the norm of the vector.

Since the units for force and moment are different, we treat the distance calculation in 6-dimensional space presented by Eq. (46) in a slightly different way, in which the last three components corresponding to the moment are divided by the radius of the MP. In practice, we multiply the last three columns of $\mathbf{A}_{\mathrm{w}_p}$ and divide the last three components of $\mathbf{c}_{g,p}$ by r_p when calculating ζ such that the different directions of capacity margin in the 6-dimensional space are expressed using the same unit (Newton). As a result, the capacity margin can be used to quantify the wrench

capability of the FPR in a given robot configuration. It depicts the robot capability in compensating any external wrenches exerted to the MP when the robot is working in its static equilibrium.

Additionally, similar quantities can be defined for finding the admissible range of external force or moment that can be exerted on the MP while compensating respectively the gravity moment or force exerted on the platform. This can be done by considering additional equality constraints in AWS defined by Eq. (43) corresponding to the equilibrium of ${}^P\boldsymbol{\tau}_p = -[\mathbf{c}_{g,p}(4), \mathbf{c}_{g,p}(5), \mathbf{c}_{g,p}(6)]^T$ for analyzing admissible external force or $\mathbf{f}_p = -[\mathbf{c}_{g,p}(1), \mathbf{c}_{g,p}(2), \mathbf{c}_{g,p}(3)]^T$ when admissible external moment is analyzed. Then the capacity margin for external force/moment, denoted by ζ_f and ζ_τ, can be computed based on the shortest distance from any force/moment to all the facets of the newly obtained 3-dimensional space.

We additionally remark that when finding the AWS of the MP and calculating its capacity margins, we assume that the thrust force vector of the quadrotors can be generated within the space defined by the augmented ATS. The transient phase of each thrust vector within the individual ATS is however neglected in our static equilibrium analysis. It should be noted that this assumption is realistic as the rotational dynamics of quadrotors are much faster than the dynamics response of the MP.

4 CASE STUDIES

In this section, several case studies are conducted following the procedure of determining the available wrench set (AWS) of the moving-platform (MP) presented in Section 3. The model of the FPR composed of three limbs connected with quadrotors is considered, for which $n = 3$. The constant parameters are given in Table 1, which take exactly the same values as the working prototype of the FPR (see Fig. 1) on which we evaluate the performance in the real-world scenario. The quadrotors used in the FPR are considered homogeneous with the same actuation limits given as $f_{max} = 25$ N and $\gamma_{max} = 35°$. The thrust limit corresponds to the value measured during the real flight of the quadrotor system we used, while the inclination angle limit was arbitrarily chosen as a sufficiently large value to ensure a stable but not overly aggressive flight in the FPR system.

Figure 6 shows a discretized ATS with 17 vertices, for $f_{max} = 25$ N and $\gamma_{max} = 35°$. By increasing the number of discretized vertices, the resulting ATS is closer to the continuous ATS mathematically described in Eq. (11). However, the computation complexity explodes at the same time. A good compromise between the computation time and discretization precision should be considered when selecting the number of vertices to represent the ATS.

Parameter	Value	Unit	Parameter	Value	Unit
m_p	0.215	[kg]	m_{d3}	1.020	[kg]
m_l	0.066	[kg]	l	1.043	[m]
m_{d1}	1.025	[kg]	r_p	0.127	[m]
m_{d2}	1.045	[kg]	r_l	0.599	[m]

Table 1: Constant geometric parameters in the case studies.

As the calculation of the AWS depends on the robot configuration, i.e., the orientation of the MP and the angles of the limbs, the following cases are considered:

1. Two orientation cases of the MP: flat orientation (i.e., $\mathbf{q}_p = [1, 0, 0, 0]^T$) and an inclined orientation with $\mathbf{q}_p = [0.973, 0.085, 0.216, -0.019]^T$ corresponding to approximately $\phi_p = 10°$ and $\vartheta_p = 25°$.
2. Three sets of the leg angles (i.e., revolute joint angles of the legs): the angles are selected to be identical for all three legs and range within $\{25°, 45°, 65°\}$.

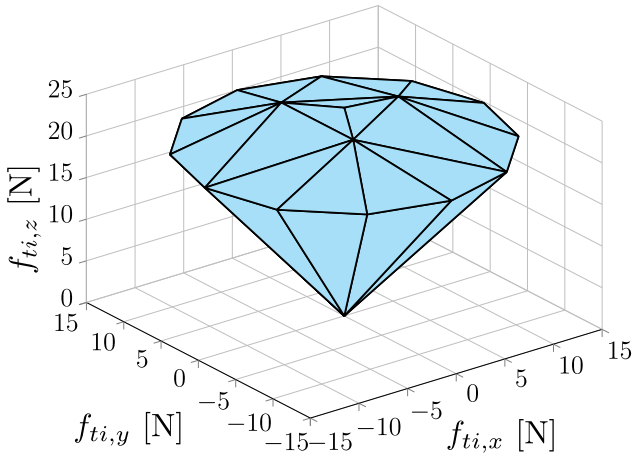

Fig. 6: ATS discretized with 17 vertices

4.1 Analysis of AWS

For a given robot configuration, the generalized AWS is firstly calculated, mapped from the augmented ATS $\mathcal{T}$ defined in Eq. (13) using the wrench matrix given by Eq. (35). We then are able to construct the AWS by further considering the additional constraints introduced by the static equilibrium of each limb around the axis of the revolute joint. Recall that this AWS depicts the admissible range of wrench exerted on the MP without considering the constant wrench due to the masses of the limbs that is transmitted to the MP, i.e., the admissible range of $\mathbf{w}'_p = \mathbf{w}_p - \mathbf{c}_{g,l/p}$.

Fig. 7 demonstrates the AWS of the MP with two different platform orientations. The 6-dimensional AWS is projected into the 3-dimensional space with respectively the first three (force) and last three (moment) components of $\mathbf{w}'_p$. The available force and moment sets of the MP are separately visualized, however it doesn't mean that they are decoupled. It can be seen that with leg angles being increased from $25°$ to $65°$, the volume of the AWS of the MP increases. This is consistent with the fact that the constant moment needed to balance the limb in its equilibrium is smaller when the leg angles increase, i.e., the leg configuration adopts a narrow form, with the legs positioned closer to being perpendicular to the plane of the platform. Therefore, the range of the admissible force and moment transmitted to the MP is relatively larger.

The available force sets demonstrated in Fig. 7a and 7c show that the maximum admissible force along z axis is always the same regardless of the platform's orientation, as the force is expressed in $\mathfrak{F}_0$. When the MP is inclined, it can be noticed that the form of admissible force spaces is distorted along the normal direction of the MP in $\mathfrak{F}_0$. As for the admissible moment exerted to the MP, when the value of leg angles is relatively small, there is more availability on the moment generated around the z axis of the platform. It should be further remarked that the visualized force and moment spaces corresponding to the same AWS are coupled. A force vector located within the available force set associates with a corresponding point in the available moment space. Therefore, the associated 3-dimensional force and moment located within the AWS are simultaneously exerted to the MP, which are available considering the actuation limits of quadrotors.

4.2 Analysis of Capacity Margin

The above-presented analysis only consists in qualitative results of the available wrench exerted on the MP. It is also important to quantitatively study the wrench capability by leveraging the notion of capacity margin in the static equilibrium condition. This metric allows to quantify the maximum admissible range of the wrench that can be exerted to the MP in any direction, with a given robot configuration. It helps determine the feasible manipulation force and moment that the MP can exert to the external environment, or the MP can resist against an external disturbance.

As explained in Section 3.5, the capacity margin of the robot can be computed by finding the minimum distance from a wrench that balances the constant wrench of the MP, $\mathbf{c}_{g,p}$, to all the facets of the AWS, using the formula Eq. (46). In addition, the capacity margins for the admissible force and moment of the platform can be separately analyzed. As discussed in Section 3.5, this can be done by considering an additional static equilibrium condition

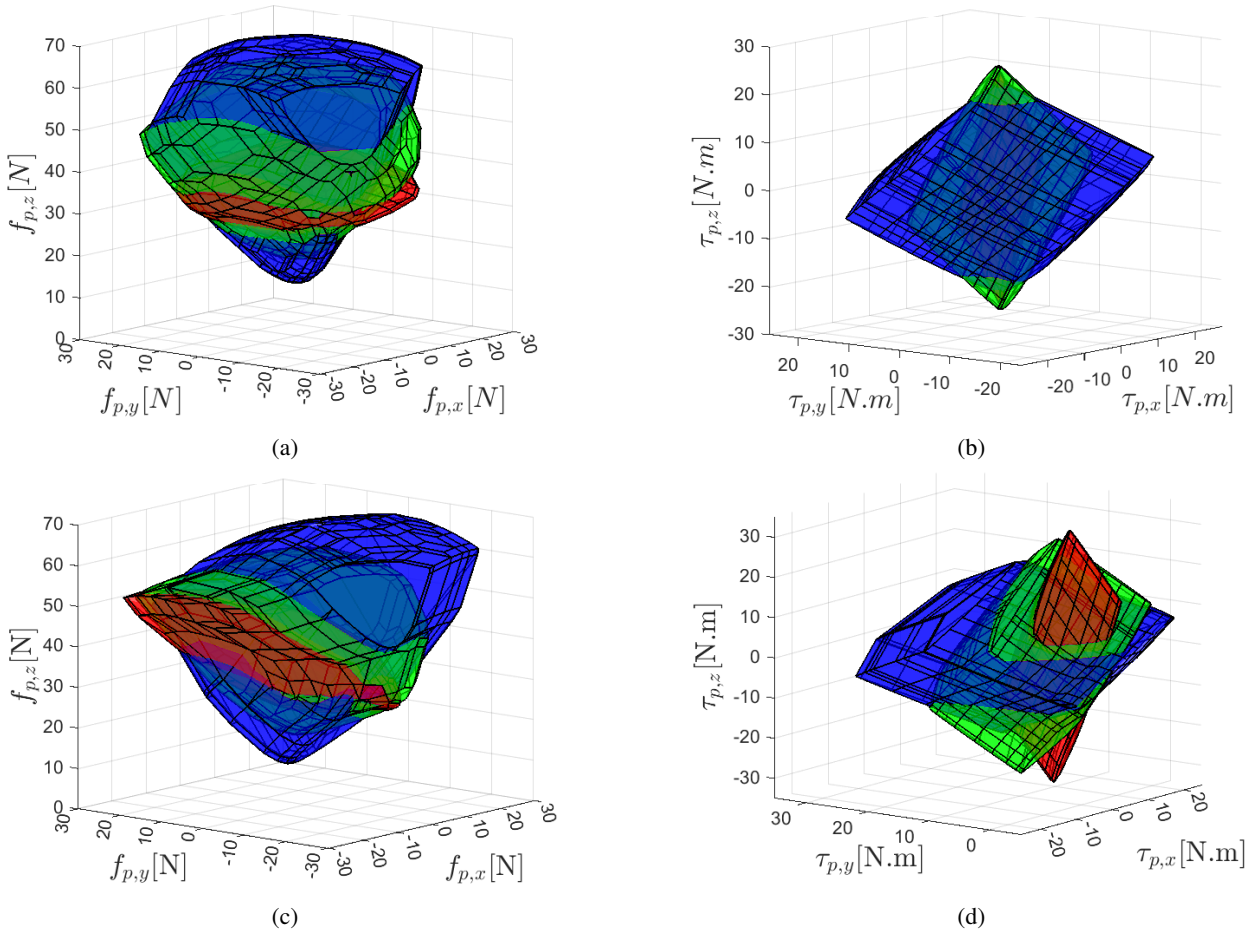

Fig. 7: Available wrench sets of the MP in different platform orientation cases. (a) and (b): available force and moment of the MP when its orientation is flat; (c) and (d): available force and moment of the MP with an inclined orientation. Note that the available forces are expressed in $\mathfrak{F}_0$ while the available moments are in $\mathfrak{F}_p$. The leg angles are identical for three limbs, with the spaces visualized in different colors for different leg angle values (red: $25°$, green: $45°$, blue: $65°$).

of the MP, respectively written as ${}^P\boldsymbol{\tau}_p = -[\mathbf{c}_{g,p}(4), \mathbf{c}_{g,p}(5), \mathbf{c}_{g,p}(6)]^T$ and $\mathbf{f}_p = -[\mathbf{c}_{g,p}(1), \mathbf{c}_{g,p}(2), \mathbf{c}_{g,p}(3)]^T$. The capacity margins for the force and moment of the MP (i.e., ζ_f and ζ_τ) are then computed based on the same calculation method of Eq. (46), in which the constraint matrix and vector are those of the newly-obtained available force set (AFS) or available moment set (AMS) that are now decoupled. ζ_f and ζ_τ define the admissible range of force and moment exerted on the platform when all the static equilibrium conditions (including that of the platform) are satisfied. For instance, the capacity margin for platform force is analyzed when the constant moment of the platform due to its mass is balanced as well as the limbs are maintained in their static equilibrium conditions.

Figure 8 shows an example of the AFS and AMS and the calculation of their capacity margins for leg angles being $45°$ with the flat orientation of the MP. Table 2 summarizes the capacity margins under the robot configuration cases studied in this section. It can be noticed that in both orientation cases, the capacity margin ζ is larger when the leg angles are 45°. With leg angles being increased to 65°, although the qualitative results show that the volume of the AWS is larger (see Section 4.1), the robot can exert less amount of wrench on the MP or is less stable facing with external disturbances, as demonstrated by the capacity margins.

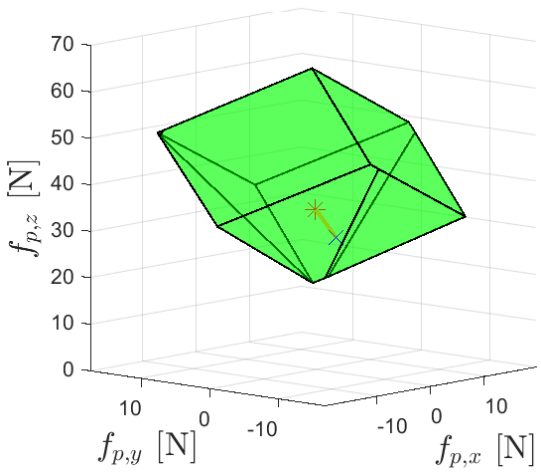

(a) Available force set and its capacity margin analyzed under the condition of ${}^{P}\boldsymbol{\tau}_p = -\mathbf{c}_{g,p}(4{:}6)$

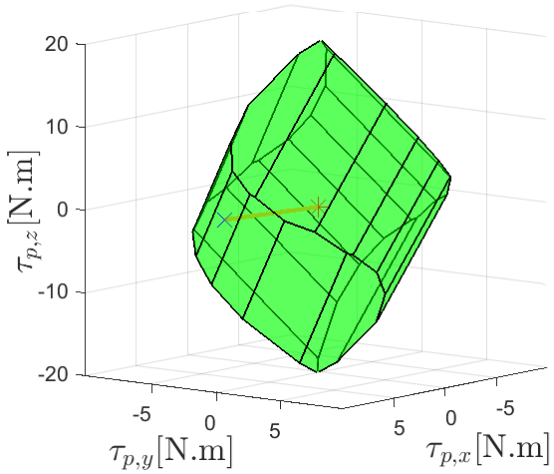

(b) Available moment set and its capacity margin analyzed under the condition of $\mathbf{f}_p = -\mathbf{c}_{g,p}(1{:}3)$

Fig. 8: Available force and moment sets of the MP in static equilibrium with the flat orientation and the leg angles being $45°$. Note that the force and moment that compensate the gravity wrench (i.e., $-\mathbf{c}_{g,p}$) are respectively shown by the red star points, and the capacity margins are demonstrated by the straight lines in orange defining the distance to the closest facet with projected points shown in blue cross.

$\boldsymbol{\theta}$	Flat orientation			Inclined orientation		
	ζ[N]	ζ_f[N]	ζ_τ[N.m]	ζ[N]	ζ_f[N]	ζ_τ[N.m]
25°	7.80	7.94	5.18	2.34	2.38	1.64
45°	7.83	7.82	6.58	3.29	3.34	2.53
65°	6.09	6.14	5.99	1.08	1.09	0.91

Table 2: Capacity margins of the AWS corresponding to the robot configurations where the leg angles $\boldsymbol{\theta}$ range within 25°, 45° and 65° cases, with two different orientations of the MP.

4.3 Analysis of Optimal Leg Configuration

Apart from the above-mentioned analysis based on the selected robot configuration cases, we can also leverage the notion of capacity margin to find the optimal leg configuration (i.e., the angles of the limbs), with a given platform orientation, that could maximize the capacity margins and thus provide the greatest range of admissible wrench exerted to the MP. We compute the capacity margins by varying the leg angles (having the identical value) within the range of $(0, 90)°$ with intervals of $1°$. Note that the range of leg angles excludes two extremity cases (i.e., $\theta_i = 0°$ and $\theta_i = 90°$) which pertain to singularity.

Fig. 9 shows the evolution of capacity margins as a function of leg angles in two orientations of the MP. Note that when the capacity margin is zero, the robot is not even able to resist the constant wrench of gravity and maintain the static equilibrium, which thus refers to a unstable leg configuration. Apparently, when the orientation of the MP is inclined, the span of feasible leg configuration is smaller than the flat orientation case. It can also be seen that the form of ζ, that considers the overall capacity margin of the force and moment exerted on the platform, is similar to that of ζ_f. They reach the maximum value approximately at the same leg angle value, whereas the capacity margin of moment ζ_τ reaches its maximum when the leg angle has a slightly larger value. Considering the values of ζ, we can obtain the admissible range of leg angles and the optimal leg angle according to the two orientation cases studied in this paper, summarized in Table 3.

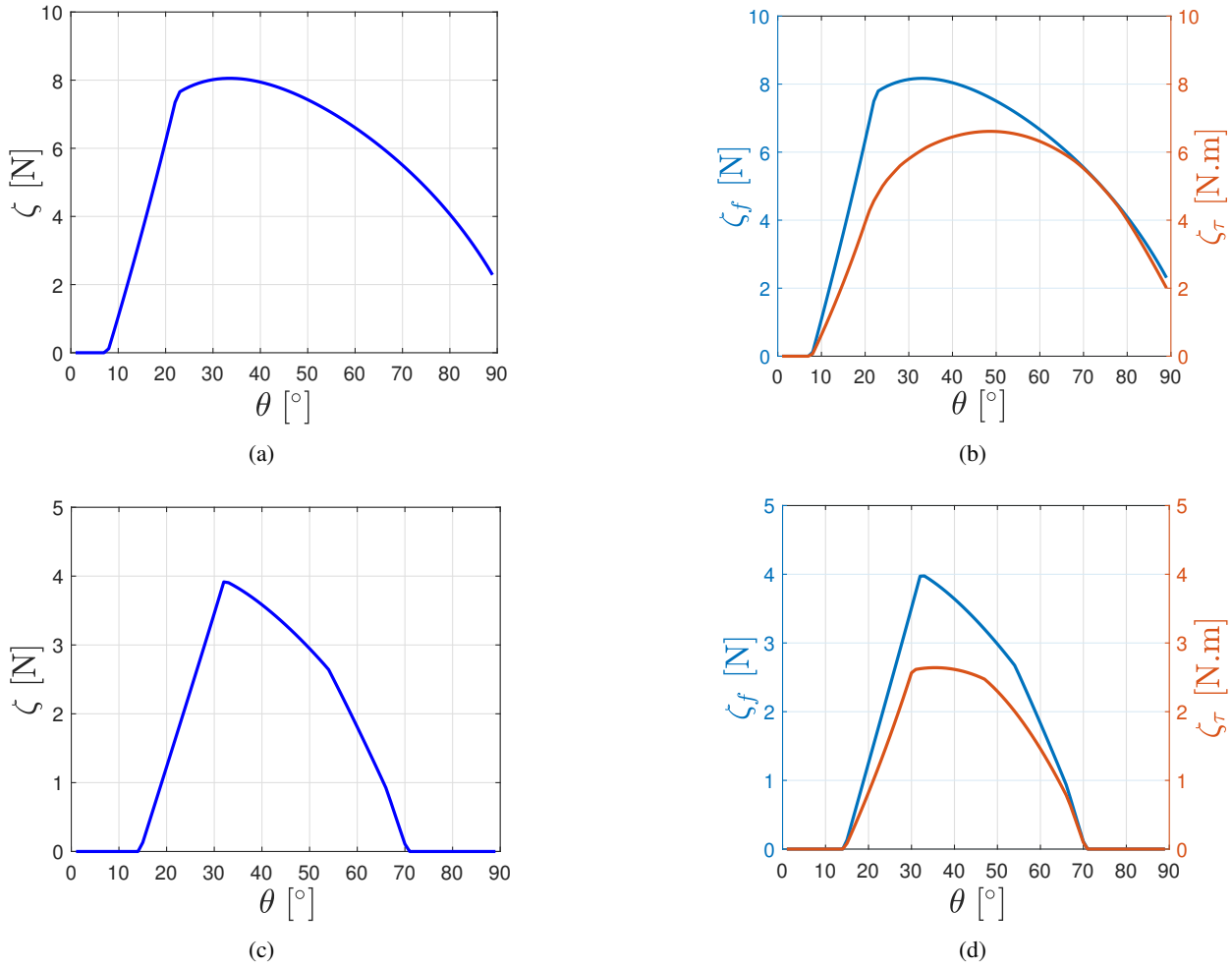

Fig. 9: Capacity margins as a function of the leg angles for two different orientations of the MP. (a) and (b): flat orientation, (c) and (d): inclined orientation.

$\mathbf{q}_p$	Admissible $\boldsymbol{\theta}$ [°]	Optimal $\boldsymbol{\theta}$ [°]	ζ [N]
Flat	[8, 90)	34	8.05
Inclined	[15, 70]	32	3.92

Table 3: Optimal leg configuration with maximum capacity margin in two platform orientation cases.

5 SIMULATION AND EXPERIMENTAL VALIDATION

We validate the wrench capability analysis detailed in the above sections both in simulation and on a real robot (as shown in Fig. 10). For simulation, we built up the model of the FPR under ROS-Gazebo environment based on PX4-autopilot quadrotor simulator [25], which allows a SITL (simulation-in-the-loop) implementation and validation. The quadrotor simulator has a chain of simulated sensors with realistic noises that represent the behavior as close as possible to the real-world system. For the real-world implementation as shown in Fig. 10b, we used customized Crazy2Fly-frame quadrotors, equipped with PX4 autopilot and Pixhawk 5 flight controller. The FPR architecture was customized using a platform in aluminium alloy, carbon fiber legs and 3D-printed connection parts, of which the

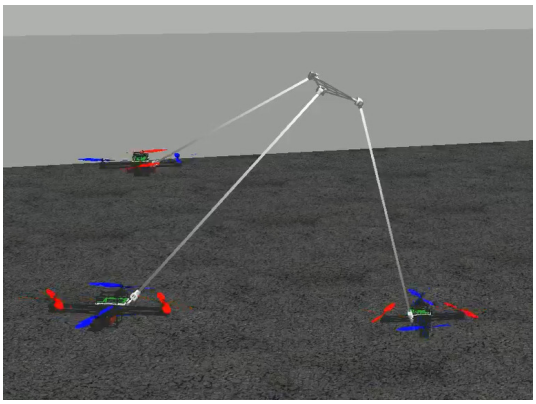

(a) Simulation validation in ROS/Gazebo environment.

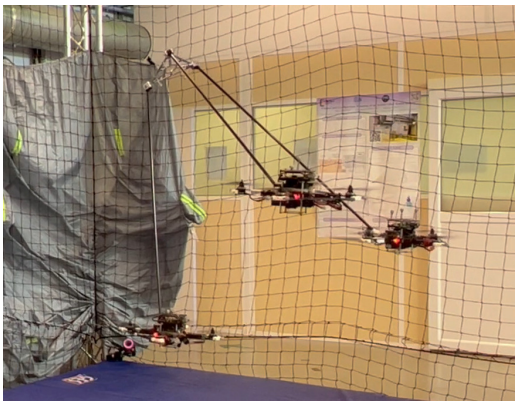

(b) Experimental validation performed with the FPR prototype.

Fig. 10: Simulation and experimental environments for validating the wrench capability analysis of the FPR.

constant parameters are given in Table 1. As for controlling the FPR to track a prescribed trajectory that involves leg angle changes in different orientations, we utilized the basic PID-based dynamic controller. For more implementation details, readers are referred to [20]. A video demonstration is available here[1].

5.1 Simulation Analysis

We first validate the wrench capability analysis by verifying the stability of the FPR system with the leg angles being evolved in the admissible range under two studied platform orientation cases. As the capacity margin decreases (shown in Fig. 9), the robot is less capable of maintaining its configuration in static equilibrium, which makes it more vulnerable to the external disturbances, eventually resulting in the failure of the flight when the capacity margin is approaching zero. To avoid potential crashes in a real-world flight that may break down the robot, we only conduct this analysis in simulations.

Figures 11 and 12 demonstrate the tracking of desired robot configuration and the evolution of capacity margins, respectively when the platform orientation is flat and inclined. It can be noticed that the curves of capacity margins ζ and ζ_f are approximately overlapped, indicating that the overall capacity margin of the platform is mainly dominated by the capability of force. This could be explained by the fact that the radius of the platform is relatively small, it thus reduces the moment factor when combining the force and moment capacity margins into ζ. When the leg angle values are evolved and approach the admissible range limits detailed in Table 3, the capacity margins decrease dramatically to zero, which results in both flight instability, as seen in oscillatory behavior of robot configuration tracking at the last moments, and crashes indicated by black dashed lines that eventually happened in simulations. It should however be remarked that in the case of flat platform orientation, there is no upper bound for the admissible leg angles. The system is static-equilibrium-wise stable as long as the leg angle values are smaller than 90°, which corresponds to a singularity condition. This can be visualized in Fig.11d that the capacity margins have been stabilized around a value much greater than zero. The crash still happened at the end of the flight, mainly due to the numerical instability of the controller when the leg angles are close to the singularity conditions.

5.2 Experimental Validation

We have also conducted real-world experiments to validate the proposed wrench analysis of the FPR. To do that, we chose two orientation cases along with three different sets of leg angles analyzed in Section 4. For each of all configurations, we flew the FPR for hovering and tracking the desired configuration in front of a fan that generated winds perturbing the system. The capacity margin differs with the robot configuration. For both orientation cases the leg configuration with the angle values being 45° is the more favorable in terms of capacity margins. Therefore, the tracking performance of the desired configuration is supposed to be better with favorable leg angles being 45°.

[1] https://youtu.be/tCJ4g8VKxbE

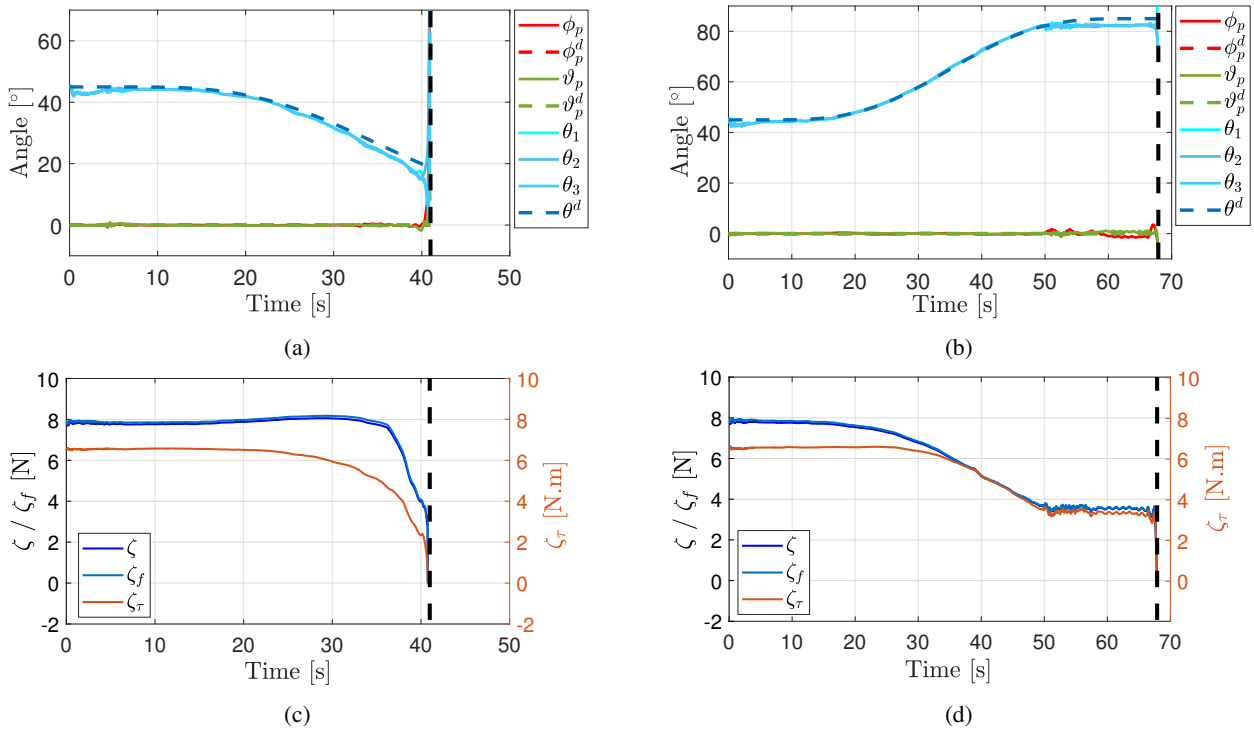

Fig. 11: Flight stability analysis in simulation when evolving the leg angles with the flat platform orientation. (a) and (b): tracking of the robot configuration, with desired values shown in dashed lines and actual values in solid curves, (c) and (d): capacity margins. Note that (a) and (c) are for the flight when the leg angles are being decreased (to a wide configuration where the legs are positioned closer to being parallel with the plane of the platform), whereas (b) and (d) are for the flight when the leg angles are being increased (to a narrow configuration).
The black dashed lines indicate the time when the flight has crashed.

$\boldsymbol{\theta}^d$	Flat orientation			Inclined orientation		
	ϕ_p	ϑ_p	mean $\boldsymbol{\theta}$	ϕ_p	ϑ_p	mean $\boldsymbol{\theta}$
25°	11.9	6.6	4.4	16.0	8.1	5.9
45°	**4.0**	**4.3**	**2.2**	**3.8**	**6.4**	**1.5**
65°	4.1	18.2	5.8	4.5	16.5	5.2

Table 4: Root-mean-square (RMS) error (in degrees) of the tracking of desired robot configuration under the condition of different platform orientations and leg angles.

Table 4 summarizes the RMS error of the tracking of desired configuration in different scenarios including three sets of desired leg angle values and two different orientations. It is apparently shown in both orientation cases that the tracking performance is better and thus the robot is more resilient in front of perturbations when performing with leg angles being 45° compared to other angle cases. By cross validating with the capacity margins given in Table 2, the coherence between the wrench capacity and the performance of the desired configuration tracking can be well identified, indicating that the analysis presented in this paper could be of interest in terms of determining the optimal leg configuration in real flight. It should however be remarked that this experimental analysis is done quite qualitatively, because in real flight there are a lot of other factors affecting the experimental results, such as

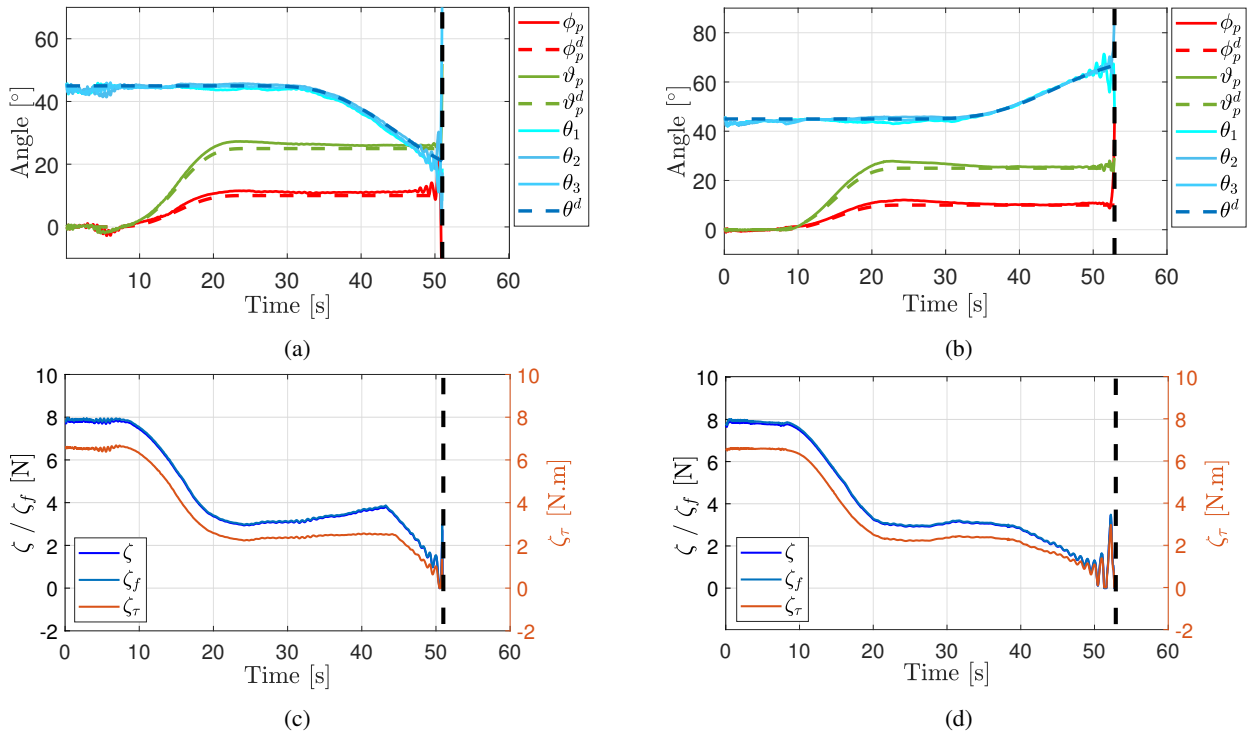

Fig. 12: Flight stability analysis in simulation when evolving the leg angles with the inclined platform orientation. The meanings of the sub-figures are the same as represented in Fig. 11.

uncertainties in real thrust generated by the quadrotor, errors in robot pose estimation, and the noise of the onboard sensors used for achieving the flight control.

6 CONCLUSION

This paper studied the wrench capability analysis of a cooperative multi-UAV parallel robot, known as Flying Parallel Robot (FPR). The latter involves multiple quadrotors supporting a moving-platform (MP) by rigid links. The notion of available thrust set (ATS) that depicts the actuation limits of quadrotors and available wrench set (AWS) that determines the wrench capability of the MP are introduced and calculated. Capacity margins of the resulting AWS quantitatively illustrate the wrench capability in any specific robot configuration. Based on the quantitative analysis, the admissible range of the leg angle values is derived with a given platform orientation configuration, which further allows to determine the optimal leg configuration that maximizes the wrench capability of the robot. Future work can extend this analysis conducted at quasi-static equilibrium to consider the dynamics of the system. The synthesized wrench analysis may be applied to the planning of optimal leg configuration that could be done off-line or online when the robot is performing a manipulation task to ensure it is wrench capable. The analysis method can also be used in an optimal design of the FPR architecture, in which the wrench capability of the system can be considered.

ACKNOWLEDGEMENTS

This work has been partially supported by ROBOTEX 2.0, the French Infrastructure in Robotics under the grants ROBOTEX (EQUIPEX ANR-10-EQPX-44-01) and TIRREX (EQUIPEX+ grant ANR-21-ESRE-0015) funded by the French Program France 2030.

REFERENCES

[1] Gouttefarde, M., Daney, D., and Merlet, J. P., 2011, "Interval-analysis-based determination of the wrench-feasible workspace of parallel cable-driven robots," *IEEE Trans. Robot.,* **27**(1), pp. 1–13.

[2] Bouchard, S., Gosselin, C., and Moore, B., 2010, "On the ability of a cable-driven robot to generate a prescribed set of wrenches," *J. Mech. Robot.,* **2**(1), pp. 1–10.

[3] Carpentier, J., Budhiraja, R., and Mansard, N., 2017, "Learning feasibility constraints for multi-contact locomotion of legged robots," In 2017 Robotics: Science and Systems (RSS), Vol. 13.

[4] Fernbach, P., Tonneau, S., and Taix, M., 2018, "CROC: Convex Resolution of Centroidal Dynamics Trajectories to Provide a Feasibility Criterion for the Multi Contact Planning Problem," In 2018 IEEE International Conference on Intelligent Robots and Systems (IROS), pp. 8367–8373.

[5] Orsolino, R., Focchi, M., Mastalli, C., Dai, H., Caldwell, D. G., and Semini, C., 2018, "Application of wrench-based feasibility analysis to the online trajectory optimization of legged robots," *IEEE Robotics and Automation Letters,* **3**(4), pp. 3363–3370.

[6] Carpentier, J., and Mansard, N., 2018, "Multi-contact Locomotion of Legged Robots," *IEEE Transactions on Robotics,* **34**(6), pp. 1441–1460.

[7] Aceituno-Cabezas, B., Mastalli, C., Dai, H., Focchi, M., Radulescu, A., Caldwell, D. G., Cappelletto, J., Grieco, J. C., Fernández-López, G., and Semini, C., 2018, "Simultaneous Contact, Gait, and Motion Planning for Robust Multilegged Locomotion via Mixed-Integer Convex Optimization," *IEEE Robotics and Automation Letters,* **3**(3), pp. 2531–2538.

[8] Orsolino, R., Focchi, M., Caron, S., Raiola, G., Barasuol, V., G. Caldwell, D., and Semini, C., 2020, "Feasible Region: An Actuation-Aware Extension of the Support Region," *IEEE Transactions on Robotics,* **36**(4), pp. 1239–1255.

[9] Miller, A. T., and Allen, P. K., 2004, "Grasp it! A Versatile Simulator for Robotic Grasping," *IEEE Robotics and Automation Magazine*(December).

[10] Borst, C., Fischer, M., and Hirzinger, G., 2004, "Grasp Planning: How to Choose a Suitable Task Wrench Space," In 2004 IEEE International Conference on Robotics and Automation (ICRA), pp. 319–325.

[11] Krug, R., Lilienthal, A. J., Kragic, D., and Bekiroglu, Y., 2016, "Analytic grasp success prediction with tactile feedback," In 2016 IEEE International Conference on Robotics and Automation (ICRA), IEEE, pp. 165–171.

[12] Michael, N., Fink, J., and Kumar, V., 2010, "Cooperative Manipulation and Transportation with Aerial Robots," In *Robotics: Science and Systems V*. The MIT Press, 07.

[13] Erskine, J., Chriette, A., and Caro, S., 2019, "Wrench Analysis of Cable-Suspended Parallel Robots Actuated by Quadrotors UAVs," *ASME Journal of Mech. and Robot.,* **11**(2), p. 020909.

[14] Sanalitro, D., Savino, H. J., Tognon, M., Cortés, J., and Franchi, A., 2020, "Full-Pose Manipulation Control of a Cable-Suspended Load with Multiple UAVs under Uncertainties," *IEEE Robot. Autom. Lett.,* **5**(2), pp. 2185–2191.

[15] Nguyen, H. N., Park, S., Park, J., and Lee, D., 2018, "A Novel Robotic Platform for Aerial Manipulation Using Quadrotors as Rotating Thrust Generators," *IEEE Trans. Robot.,* **34**(2), pp. 353–369.

[16] Li, Z., Bégoc, V., Chriette, A., and Fantoni, I., 2022, "Wrench Capability Analysis and Control Allocation of a Collaborative Multi-Drone Grasping Robot," *Journal of Mechanisms and Robotics,* **15**(2), 06.

[17] Six, D., Briot, S., Chriette, A., and Martinet, P., 2018, "The Kinematics, Dynamics and Control of a Flying Parallel Robot with Three Quadrotors," *IEEE Robot. Autom. Lett.,* **3**(1), pp. 559–566.

[18] Liu, S., Erskine, J., Chriette, A., and Fantoni, I., 2021, "Decentralized Control and Teleoperation of a Multi-UAV Parallel Robot Based on Intrinsic Measurements," In 2021 IEEE International Conference on Intelligent Robots and Systems (IROS), pp. 6306–6312.

[19] Liu, S., Fantoni, I., Chriette, A., and Six, D., 2022, "Wrench estimation and impedance-based control applied to a flying parallel robot interacting with the environment," *IFAC-PapersOnLine,* **55**(14), pp. 151–157.

[20] Liu, S., Fantoni, I., and Chriette, A., 2024, "Decentralized control and state estimation of a flying parallel robot interacting with the environment," *Control Engineering Practice*(144), p. 105817.

[21] Rasheed, T., Long, P., and Caro, S., 2020, "Workspace of Mobile Cable-Driven Parallel Robots," *ASME Journal of Mech. and Robot.,* **12**(3), p. 031009.

[22] Gouttefarde, M., and Krut, S., 2010, "Characterization of parallel manipulator available wrench set facets," In Advances in Robot Kinematics: Motion in Man and Machine, J. Lenarcic and M. M. Stanisic, eds., Springer

Netherlands, pp. 475–482.
[23] Herceg, M., Kvasnica, M., Jones, C. N., and Morari, M., 2013, "Multi-parametric toolbox 3.0," In 2013 European Control Conference (ECC), pp. 502–510.
[24] Guay, F., Cardou, P., Cruz Ruiz, A. L., and Caro, S., 2014, "Measuring How Well a Structure Supports Varying External Wrenches," *New Advances in Mechanisms, Transmissions and Applications Mechanisms and Machine Science,* **17**, pp. 385–392.
[25] PX4-autopilot simulation package Web Page (PX4-Autopilot) available at https://docs.px4.io/v1.12/en/simulation/gazebo.

APPENDIX: CONVEX POLYTOPE

A polytope is a convex set contained in a n-dimensional Euclidean space $\mathbb{R}^n$ given by a finite number of closed segments, which can be represented either using a convex set of vertices (so-called V-representation) or as the intersection of half-spaces and hyperplanes (named as H-representation). The mathematical expression of a convex set defined respectively by two representations is given as follows:

V-representation:

$$\mathcal{S} = \left\{ \mathbf{x} \in \mathbb{R}^n \;\middle|\; \mathbf{x} = \sum_{k=1}^{n_v} \lambda_k \mathbf{v}_k, \;\; \lambda_k > 0, \; \sum_{k=1}^{n_v} \lambda_k = 1 \right\} \tag{47}$$

where $\mathbf{v}_k \in \mathbb{R}^n$ are the vertices, n_v is the total number of the vertices.

H-representation:

$$\mathcal{S} = \left\{ \mathbf{x} \in \mathbb{R}^n \;\middle|\; \mathbf{A}\mathbf{x} \leq \mathbf{b}, \; \mathbf{C}\mathbf{x} = \mathbf{d} \right\} \tag{48}$$

where $\mathbf{A} \in \mathbb{R}^{n \times n}$, $\mathbf{b} \in \mathbb{R}^n$ parameterize the inequality constraints for the half-spaces, and $\mathbf{C} \in \mathbb{R}^{n \times n}$, $\mathbf{d} \in \mathbb{R}^n$ represent the hyperplanes.

NOMENCLATURE

$\mathfrak{F}_0$	global reference frame with origin at point O	$\boldsymbol{\tau}_{g,li/p} \in \mathbb{R}^3$	constant moment of gravity exerted by the limb i to the MP
$\mathfrak{F}_P$	platform frame, with CoM located at point P	$\boldsymbol{\tau}_{g,li} \in \mathbb{R}^3$	constant moment of gravity exerted around the revolute joint of the limb i
$\mathfrak{F}_{Li}, \mathfrak{F}_{Bi}$	leg i's frame and quadrotor i's body frame, with CoMs located respectively at point A_i and B_i	$\mathbf{c}_{g,l/p} \in \mathbb{R}^6$	constant wrench of gravity exerted on the MP by all the limbs
$\mathbf{p}_p \in \mathbb{R}^3$	position of the platform in $\mathfrak{F}_0$	$\mathbf{c}_{g,p} \in \mathbb{R}^6$	constant wrench of gravity exerted on the MP
$\mathfrak{q}_p \in \mathbb{H}$	unit quaternion of the platform relative to $\mathfrak{F}_0$	$\mathbf{c}_g \in \mathbb{R}^{6+n}$	constant generalized wrench of gravity of FPR
$\phi_p, \vartheta_p, \psi_p$	roll, pitch and yaw Euler angles of the platform orientation	$\mathbf{w}_p \in \mathbb{R}^6$	wrench vector of the MP
$\boldsymbol{\theta}_l \in \mathbb{R}^n$	a vector concatenating all the leg angles θ_i	$\mathbf{w}_{g,p} \in \mathbb{R}^6$	gravity wrench vector of the MP
$r_p \in \mathbb{R}$	platform's radius (length of $\overrightarrow{PA_i}$)	$\mathbf{w} \in \mathbb{R}^{6+n}$	general wrench vector of FPR
$l, r_l \in \mathbb{R}$	leg length (length of $\overrightarrow{AiBi}$ and its CoM position (length of $\overrightarrow{AiGi}$) in $\mathfrak{F}_{Li}$	$\mathbf{w}'_p \in \mathbb{R}^6$	equivalent wrench vector of the MP excluding the gravity constant $\mathbf{c}_{g,p}$
$\mathbf{r}_{AiBi}, \mathbf{r}_{AiGi}$	3-dimensional vectors of $\overrightarrow{AiBi}$ and $\overrightarrow{AiGi}$	$\mathbf{w}' \in \mathbb{R}^{6+n}$	equivalent generalized wrench vector of FPR excluding the gravity constant $\mathbf{c}_g$
$\mathbf{r}_{PAi}$	3-dimensional vectors of $\overrightarrow{PAi}$	$\mathbf{R}_P \in SO(3)$	rotation matrix of the MP relative to $\mathfrak{F}_0$
m_p, m_l, m_{di}	mass of the MP, the leg and the quadrotor i	$\mathbf{R}_{Bi} \in SO(3)$	rotation matrix of the quadrotor i relative to $\mathfrak{F}_0$
$\mathbf{f}_{ti} \in \mathbb{R}^3$	thrust force of the i-th quadrotor expressed in $\mathfrak{F}_0$	$\mathbf{R}_{Li} \in SO(3)$	rotation matrix of leg i's frame relative to $\mathfrak{F}_0$
$f_{ti} \in \mathbb{R}$	thrust force magnitude of the i-th quadrotor	$\mathbf{S}_\tau$	moment transmission matrix of a revolute joint
$f_{max} \in \mathbb{R}$	maximum admissible thrust force of quadrotor	$\mathbf{W}_p$	wrench matrix of the MP
$\gamma_{max} \in \mathbb{R}$	maximum inclination angle of quadrotor	$\mathbf{W}_{\tau_l}$	sub-wrench matrix for the limbs
$\mathbf{f}_t \in \mathbb{R}^{3n}$	generalized vector including thrust forces of all the quadrotors	$\mathbf{W}$	generalized wrench matrix
$\mathbf{f}_p \in \mathbb{R}^3$	force exerted on the MP in $\mathfrak{F}_0$	$\mathcal{T}_i$	available thrust set of the quadrotor i
${}^p\boldsymbol{\tau}_p \in \mathbb{R}^3$	moment exerted on the MP in $\mathfrak{F}_p$	$\mathcal{W}_p$	available wrench set of the platform
$\mathbf{f}_{li/p} \in \mathbb{R}^3$	reaction force between the limb i and the MP	$\mathcal{W}'$	generalized available wrench set of the robot
$\boldsymbol{\tau}_{li/p} \in \mathbb{R}^3$	reaction moment between the limb i and the MP	$\zeta \in \mathbb{R}$	capacity margin of AWS
$\tau_{li} \in \mathbb{R}$	a virtual moment generated around the revolute joint of the limb i	$\zeta_f, \zeta_\tau \in \mathbb{R}$	capacity margins of force and moment in static equilibrium condition
$\boldsymbol{\tau}_l \in \mathbb{R}^n$	a vector concatenating virtual moments of all the limbs	$\mathbf{0}_k$	a k-dimensional column vector of zeros
$\mathbf{f}_{g,li/p} \in \mathbb{R}^3$	constant force of gravity exerted by the limb i to the MP	$\mathbf{1}_{k\times k}$	$k \times k$ identity matrix
		$\mathbf{i}, \mathbf{j}, \mathbf{k}$	unit vector of x, y, z axis of a frame

ATS	Available Thrust Set	**AWS**	Available Wrench Set
CoM	Center of Mass	**DoF**	Degree of Freedom
FPR	Flying Parallel Robot	**GAWS**	Generalized Available Wrench Set
MP	Moving-Platform	**RMS**	Root Mean Square
ROS	Robot Operating System	**UAV**	Unmanned Aerial Vehicle